HHS Public Access

Author manuscript

Cell Stem Cell. Author manuscript; available in PMC 2017 August 07.

Published in final edited form as:

Cell Stem Cell. 2016 February 04; 18(2): 214–228. doi:10.1016/j.stem.2015.11.001.

The *Dlk1-Gtl2* Locus Preserves LT-HSC Function by Inhibiting the PI3K-mTOR Pathway to Restrict Mitochondrial Metabolism

Pengxu Qian[1], **Xi C. He**[1], **Ariel Paulson**[1], **Zhenrui Li**[1,2], **Fang Tao**[1,2], **John M. Perry**[1], **Fengli Guo**[1], **Meng Zhao**[1], **Lei Zhi**[3], **Aparna Venkatraman**[4], **Jeffrey S. Haug**[1], **Tari Parmely**[1], **Hua Li**[1], **Rick T. Dobrowsky**[5], **Wen-Xing Ding**[6], **Tomohiro Kono**[7], **Anne C. Ferguson-Smith**[8], and **Linheng Li**[1,2,*]

[1]Stowers Institute for Medical Research, Kansas City, MO 64110, USA

[2]Department of Pathology and Laboratory Medicine, University of Kansas Medical Center, Kansas City, KS 66160, USA

[3]Department of Immunology, Tianjin Key Laboratory of Cellular and Molecular Immunology, Key Laboratory of Immuno Microenvironment and Disease of the Educational Ministry, Tianjin Medical University, Tianjin, P.R. China

[4]Centre for Stem Cell Research, Christian Medical College, Vellore, 632002, India

[5]Department of Pharmacology and Toxicology, University of Kansas, Lawrence, KS 66045, USA

[6]Department of Pharmacology, Toxicology and Therapeutics, University of Kansas Medical Center, Kansas City, KS 66160, USA

[7]Department of Bioscience, Tokyo University of Agriculture, Tokyo 156-8502, Japan

[8]Department of Genetics, University of Cambridge, Downing Street, Cambridge CB2 3EG, UK

SUMMARY

The mammalian imprinted *Dlk1-Gtl2* locus produces multiple non-coding RNAs (ncRNAs) from the maternally inherited allele, including the largest miRNA cluster in the mammalian genome. This locus has characterized functions in some types of stem cell, but its role in hematopoietic stem cells (HSCs) is unknown. Here, we show that the *Dlk1-Gtl2* locus plays a critical role in preserving long-term repopulating HSCs (LT-HSCs). Through transcriptome profiling in 17 hematopoietic cell types, we found that ncRNAs expressed from the *Dlk1-Gtl2* locus are

*Correspondence: lil@stowers.org.

ACCESSION NUMBERS

The accession numbers for the raw datasets reported in this paper are ArrayExpress: E-MTAB-2923, ArrayExpress: E-MTAB-3079 (mRNA-seq), and ArrayExpress: E-MTAB-3080 (small RNA-seq).

SUPPLEMENTAL INFORMATION

Supplemental Information for this article includes seven figures, seven tables, and Supplemental Experimental Procedures and can be found with this article online at http://dx.doi.org/10.1016/j.stem.2015.11.001.

AUTHOR CONTRIBUTIONS

P.Q. performed experiments, analyzed data, and wrote the manuscript. X.C.H. helped perform transplantations and RNA-seq. A.P. and H.L. performed bioinformatics analysis. Z.L., F.T., J.M.P., F.G., M.Z., L.Z., A.V., J.S.H., T.P., R.T.D., and W.X.D. helped perform part of the experiments. T.K. and A.C.F-S. contributed mouse lines. L.L. directed the overall project and co-wrote the manuscript. All authors contributed to reading and editing the manuscript.

predominantly enriched in fetal liver HSCs and the adult LT-HSC population and sustain long-term HSC functionality. Mechanistically, the miRNA mega-cluster within the *Dlk1-Gtl2* locus suppresses the entire PI3K-mTOR pathway. This regulation in turn inhibits mitochondrial biogenesis and metabolic activity and protects LT-HSCs from excessive reactive oxygen species (ROS) production. Our data therefore show that the imprinted *Dlk1-Gtl2* locus preserves LT-HSC function by restricting mitochondrial metabolism.

In Brief

Qian and colleagues show that ncRNAs expressed from the imprinted locus *Dlk1-Gtl2* maintain fetal liver and adult LT-HSCs through multiplexed inhibition of PI3K-mTOR signaling that in turn keeps mitochondrial biogenesis and metabolic activity in check.

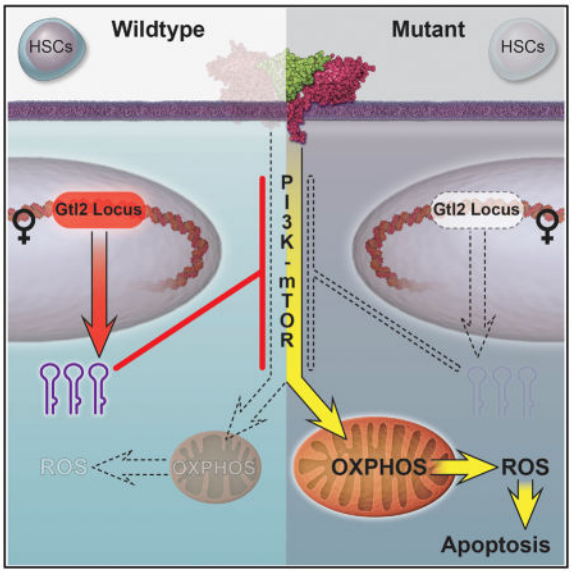

INTR ODUCTION

Homeostasis in hematopoiesis requires a balance between stem cell maintenance and action to prevent bone marrow (BM) from exhaustion or overgrowth (Li and Clevers, 2010; Wilson et al., 2008). Cell-cycle status is essential for regulation of this balance, by which long-term (LT)-HSCs are preserved in a quiescent state for maintenance whereas short-term (ST)-HSCs and multipotent progenitor (MPP) cells are fast cycling for increasing cell mass and further differentiation (Yang et al., 2005). Previous studies reported that surface marker CD49b (Integrin α2) could further separate conventional LT-HSCs ($CD34^{-}Flk2^{-}Lineage^{-}Sca\text{-}1^{+}c\text{-}Kit^{+}$ [LSK]) into $CD49b^{lo}$ LT-HSCs that maintain permanent reconstituting ability and $CD49b^{hi}$ intermediate-term (IT)-HSCs that support only 6–8 months of multipotent hematopoiesis (Benveniste et al., 2010). Recent studies reported that metabolic properties are required for maintenance of different states of HSCs (Suda et al., 2011; Takubo et al., 2013), and a low mitochondrial potential correlates with HSC functionality (Simsek et al., 2010). How cell-cycle status and metabolic states are precisely controlled in HSCs remains largely unknown.

Epigenetic regulation, including ncRNAs, DNA methylation, histone modification, and chromatin remodeling, plays essential roles in orchestrating the balance between HSC maintenance and action (Cullen et al., 2014). Genomic imprinting, a unique epigenetic regulation resulting in a parent-of-origin-specific gene expression, is essential for normal mammalian development and growth (Bartolomei, 2009; Ferguson-Smith, 2011). We initiated our study on imprinting genes after seeing a differential expression of imprinted genes in HSCs (Haug et al., 2008). Systematic gene profiling conducted by several groups revealed predominant expression of imprinted genes in HSCs as well as other somatic stem cells (Berg et al., 2011; Ferrón et al., 2011; Zacharek et al., 2011). We further functionally proved that the imprinting at the *H19-Igf2* locus is essential for maintaining HSC quiescence via suppression of *Igf1r* expression by *H19*-derived miR-675 (Venkatraman et al., 2013). In addition to miRNAs, long-length non-coding RNAs (lncRNAs) (>200 nt in length) have drawn attention for their potential regulatory roles in biological processes including stem cell property (Luo et al., 2015). These efforts have sparked interest in ncRNAs; however, whether and how ncRNAs preserve LT-HSCs remains poorly understood.

In this study, we performed transcriptome profiling in 17 sub-populations of hematopoietic stem, progenitor, and mature lineage cells, and we identified exclusively expressed "fingerprint" lncRNAs unique to each cell type. We found that lncRNAs in the *Dlk1-Gtl2* locus are specifically enriched in the CD49b^{lo} LT-HSCs. The imprinted *Dlk1-Gtl2* locus contains three protein-coding genes (*Dlk1*, *Rtl1*, and *Dio3*) on the paternally inherited allele and multiple lncRNAs and small ncRNAs on the maternally inherited allele, including *Gtl2*, *Rian* (containing 22 box C/D snoRNAs), and the largest miRNA mega-cluster in mammals (*anti-Rtl1*, which contains the miR-127/miR-136 cluster with 7 miRNAs, and *Mirg*, which contains the miR-379/miR-410 cluster with 39 miRNAs). Interestingly, all the ncRNAs are regulated by a common *cis*-element and epigenetic control, resulting in a large polycistronic transcription unit (da Rocha et al., 2008; Seitz et al., 2004; Tierling et al., 2006). The *Dlk1-Gtl2* locus plays crucial roles in embryonic and adult stem cells (Ferrón et al., 2011; Lin et al., 2003; Snyder et al., 2013). However, whether the *Dlk1-Gtl2* locus functions in HSCs and its underlying mechanism are largely uncharacterized. Here, we show how the *Dlk1-Gtl2* locus preserves functionality of LT-HSCs by inhibiting the PI3K-mTOR pathway and restricting mitochondrial metabolism.

RESULTS

Unique lncRNA Fingerprints in 17 Hematopoietic Cell Types Revealed Enrichment of lncRNAs from the *Dlk1-Gtl2* Locus in CD49b^{lo} LT-HSCs

To systematically identify lncRNAs that might play a role in LT-HSCs, we isolated four hematopoietic stem and progenitor cells (HSPCs) (CD49b^{lo} LT-HSCs, CD49b^{hi} IT-HSCs, ST-HSCs, and MPPs), four committed progenitors (common lymphoid progenitor [CLP], common myeloid progenitor [CMP], granulocyte-macrophage progenitor [GMP], and megakaryocyte-erythroid progenitor [MEP]), and nine mature lineage cells (B cell, T cell, NK cell, dendritic cell, monocyte, macrophage, granulocyte, megakaryocyte, and nucleated erythrocyte) by fluorescence-activated cell sorting (FACS) from the BM of C57BL/6J mice (Figure 1A; Figures S1A–S1F; Table S1). Next, we conducted 100 bp paired-end high-

throughput RNA-seq on poly-A^+ RNA and identified reliable lncRNAs using the stringent filtering strategies as previously reported (Alvarez-Dominguez et al., 2014) (Table S2; see Supplemental Experimental Procedures). Several known HSC markers (CD150, EPCR, and ESAM) were well captured, and the markers used for FACS exhibited consistency between transcript and protein levels, supporting the high quality of our RNA-seq data (Figure S1G). Our strategies yielded 4,204 lncRNAs, 1,606 of which (38.2%) were distinct from those in Ensembl databases. We also found that 860 (20.5%) of these lncRNAs overlapped with HSC-related lncRNAs recently reported in an elegant study (Luo et al., 2015) (Figure S1H). We then removed the least expressed transcripts by setting the threshold of FPKM (fragments per kilobase of transcript per million mapped reads) at >1 in at least one sample, which yielded 1,693 expressed lncRNAs. Compared to protein-coding genes, these lncRNAs had lower expression levels (Figure S1I) but higher tissue specificity (Figure S1J, $p = 2.2 \times 10^{-16}$, Kolmogorov-Smirnov test), implying that they might play specific roles in different types of hematopoietic cells.

To investigate the ontogeny relatedness of hematopoietic cell types, we performed unsupervised hierarchical cluster analysis. The family tree analysis clearly showed that samples from HSPCs, progenitors, and lineages correlated positively, supporting the high specificity of lncRNAs (Figure 1B). We further performed principal components analysis (PCA) to measure and visualize differences among cell types. The PCA map showed CD49b^{lo} HSCs at the apex of the hematopoietic hierarchy (Figure 1C). We also observed the striking segregation of HSPCs, progenitor cells, and mature lineages, the latter of which further divided into three discrete clusters (lymphoid, myeloid, and erythroid) (Figure 1C). Together, both cluster and PCA analyses indicated that the lncRNA profiles distinguish CD49b^{lo} HSCs from other HSC subpopulations that eventually lost their functional capacity, supporting the previous report that permanently reconstituting CD49b^{lo} HSCs have the highest self-renewal ability (Benveniste et al., 2010).

We next determined the fingerprint lncRNAs in particular cell types. Based on specificity scores, we identified 461 (27.2% in 1693) fingerprint lncRNAs in 17 cell types that could be used as specific markers and might play essential roles during lineage commitment and differentiation (Figure 1D; Table S3). Only 954 of 13,775 (6.9%) protein-coding genes were identified as fingerprint genes, suggesting that lncRNAs have much higher percentages of lineage/stage-restricted gene expression. We specifically identified 12 lncRNAs enriched in CD49b^{lo} HSCs, three of which with the highest expression levels—*Gtl2*, *Rian*, and *Gm26906*—were derived from the imprinted *Dlk1-Gtl2* locus on mouse chromosome 12qF1 (Figure 1E). Intriguingly, *H19* was also enriched in CD49b^{lo} HSCs. Furthermore, our RNA-seq data revealed that all the ncRNAs expressed from the maternally inherited allele, starting from *Gtl2* to *Mirg*, were exclusively enriched in CD49b^{lo} HSCs (Figure 1F), suggesting a potential role of ncRNAs from the *Dlk1-Gtl2* locus in preserving CD49b^{lo} LT-HSCs.

Loss of Imprinting at the *Dlk1-Gtl2* Locus Led to Deficiency in Fetal Liver HSCs

Both the intergenic germline-derived differentially methylated region (*IG-DMR*) and the *Gtl2-DMR* determine reciprocal expression of ncRNAs on the maternally inherited allele and protein-coding genes on the paternally inherited allele (Lin et al., 2003; Zhou et al.,

2010). To determine the role of the *Dlk1-Gtl2* locus in HSCs, we used the genetic mutant mice with straight knockout of *IG-DMR* (Lin et al., 2003). We bred the heterozygous *IG-DMR* mice with WT mice and then performed PCR to determine allele-specific mutants with deletion of *IG-DMR* from maternally or paternally inherited allele (mat *ΔIG* or pat *ΔIG*) and their control littermates (Figures 2A and S2A). Since mat *ΔIG* embryos were lethal after E16, we used E15 embryos, at which stage HSCs are mainly located in fetal livers. To test gene expression in the *Dlk1-Gtl2* locus in fetal liver LSK cells and adult HSCs, we compared RNA-seq data from four adult HSPCs, adult LSK cells, and E15 fetal liver LSK cells. Interestingly, we found that E15 fetal liver LSK cells exhibited expression patterns of lncRNAs in the *Dlk1-Gtl2* locus similar to those of CD49b^{lo} HSCs, but not similar to those of the other adult HSPCs (Figure 2B), suggesting that the CD49b^{lo} subset of HSCs are enriched with a feature of fetal HSCs. Thus we were able to study the behaviors of HSCs isolated from E15 fetal liver and transplanted into adult recipients to reveal potential roles of the *Dlk1-Gtl2* locus in HSCs.

We next investigated the roles of the *Dlk1-Gtl2* locus in fetal liver HSCs. Consistent with a previous study (Lin et al., 2007), we observed several symptoms of anemia, including pale skin and few vessels, in the E15 mat *ΔIG* embryos (Figure S2B). Although total cell numbers in WT and *ΔIG* mutant fetal livers remained similar (Figure 2C), we indeed observed a 2-fold decrease in both frequency and absolute number of LSK cells in mat *ΔIG*, but not in pat *ΔIG*, fetal liver (Figures 2D and 2E). To assess the effect on HSCs, we used CD93 (Morrison et al., 1995) and CD38 (Randall et al., 1996) as fetal liver HSC surface markers. Flow cytometry analysis showed that both the frequency and absolute numbers of CD93^{+} HSCs, CD38^{hi} HSCs, and CD38^{lo} HSCs declined 2-fold in mat *ΔIG* fetal livers (Figures 2F–2I). However, except for an increase in the frequency of MEP and erythroid, we did not observe any change in the other progenitors and lineage cells, reflecting a relatively specific reduction in HSCs caused by loss of mat *ΔIG* (Figures S2C–S2F). We next quantified the gene expression levels of the *Dlk1-Gtl2* locus by quantitative real-time PCR in both WT and mat *ΔIG* fetal liver cells. Interestingly, we observed almost no expression in lineage cells and no change between WT and mat *ΔIG* progenitors (Figure 2J), supporting previous observations that most progenitors and lineages cells showed no difference in frequency and absolute numbers. In contrast, we observed a substantial decrease in ncRNAs expressed from the maternally inherited allele (*Gtl2*, *Rian*, and *Mirg*) and an increase in *Dlk1* (but not *Rtl1* or *Dio3*) from the paternally inherited allele in fetal liver HSCs (Figure 2J). To assess whether *Dlk1* mediates HSC deficiency in the mat *ΔIG* mouse, we crossed mat *ΔIG* females with *Tie2-cre^{+}; Dlk1$^{fl/fl}$* males and found that deletion of *Dlk1* could not fully rescue the decreased number of mat *ΔIG* fetal liver HSPCs, excluding the possibility that defective phenotype in mat *ΔIG* was due to increased *Dlk1* expression (Figure S2G).

To assess whether loss of *Gtl2* itself could lead to HSC deficiency, we used another genetic murine mutant of *ΔGtl2*, with a deletion of the first five exons of *Gtl2* and *Gtl2-DMR* (Takahashi et al., 2009). Deletion of *Gtl2* from the maternally inherited allele (mat *ΔGtl2*) caused perinatal death and repressed all the ncRNAs expressed from the maternally inherited allele, similar to the mat *ΔIG* mice (Zhou et al., 2010). Consistently, we found that HSPCs, but not progenitors and lineages, in the mat *ΔGtl2* fetal livers exhibited decreased frequency

and absolute numbers (Figures 2K, 2L, S2H, and S2I). Together, these data indicate that loss of either mat *ΔIG* or *Gtl2* per se leads to a deficiency in fetal liver HSCs.

Loss of Imprinting at the *Dlk1-Gtl2* Locus Impaired Fetal Liver HSC Long-Term Reconstitution Capacity

To characterize the functional roles of *Dlk1-Gtl2* locus in HSCs, we conducted a competitive repopulation assay by transplanting 5×10^4 or 5×10^5 whole fetal liver cells from mutants or their control littermates as donor cells (CD45.2), together with 1×10^5 recipient BM cells (CD45.1 hereafter) derived from the *Ptprc* mutant strain, into lethally irradiated recipient mice. In the 5×10^4 group, we found that overall engraftment from mat *ΔIG* was reduced 1.4-fold, 1.8-fold, and 7.1-fold in primary (1^{st}), secondary (2^{nd}), and tertiary (3^{rd}) recipients, respectively, compared to the control group (Figure 3A). Engraftment from pat *ΔIG* showed no difference (Figure S3A). Interestingly, we observed a significant myeloid lineage bias in the 2^{nd} and 3^{rd} mat *ΔIG*-transplant recipients (Figure 3A), consistent with a previous report of myeloid lineage bias associated with HSC aging and diminished total reconstitution potential (Beerman et al., 2010). In the 5×10^5 group, we observed a 2-fold decrease in the repopulation rate and a significant myeloid lineage bias from mat *ΔIG* only in the 3^{rd} recipients, but no difference in the 1^{st} or 2^{nd} recipients (Figures S3B–S3D). We next analyzed donor HSCs in the recipient mice. In the 1^{st}, 2^{nd}, and 3^{rd} recipients, the total cell numbers in BM were not affected; however, the absolute numbers of HSPCs, including $CD49b^{lo}$ HSCs, declined significantly in mat *ΔIG*, but not in pat *ΔIG*, compared to control (Figures 3B and S3E–S3K). Intriguingly, we observed a significant decrease in the ratio of $CD49b^{lo}/CD49b^{hi}$ HSCs, from 30%/70% in control to 16%/84% in mat *ΔIG*, suggesting that deletion of *IG-DMR* from maternally inherited allele resulted in a reduction in LT-HSCs (Figure 3C). Further cell-cycle analyses in both fetal liver HSCs and donor $CD49b^{lo}$ HSCs showed a decrease in the G0 phase fraction and a concomitant increase in the G1 phase fraction in mat *ΔIG* (Figures S3L and 3D). In addition, Kaplan-Meier survival analysis revealed that mice transplanted with mat *ΔIG* showed significantly reduced survival compared to controls (Figure 3E). To investigate whether impaired reconstitution capacity was due to functional defect in HSCs, we transplanted 150 sorted HSCs from WT and mat *ΔIG* fetal livers together with 2×10^5 rescue BM cells into recipient mice. We observed a striking reduction in reconstitution ability at 12 weeks posttransplantation in mat *ΔIG* compared to control (Figure 3F). Together, these results show that fetal liver cells from mat *ΔIG* mice have significantly reduced HSC numbers, accounting for reduced long-term reconstitution capacity.

To quantify functional HSCs, we further used *ΔGtl2* mice to perform limiting dilution (5×10^3, 1.5×10^4, and 5×10^4) competitive repopulating unit (CRU) assays. We observed a 2.1-fold decrease in functional HSCs in mat *ΔGtl2* mice compared to control (Figures 3G and 3H). In the 5×10^4 group, 20 weeks posttransplantation, we observed a 2.2-fold decrease in the overall engraftment and a significant myeloid lineage bias from mat *ΔGtl2* (Figure 3I). These data reveal that loss of either mat *ΔIG* or *Gtl2* per se compromises fetal liver HSC long-term reconstitution capacity.

Loss of Imprinting at the *Dlk1-Gtl2* Locus Induced Hyperactivation of the PI3K-mTOR Pathway

We next sought to elucidate the molecular mechanisms underlying HSC defects from loss of imprinting at the *Dlk1-Gtl2* locus. To this end, we performed RNA-seq in fetal liver LSK cells and identified 991 upregulated genes and 941 downregulated genes in mat *ΔIG* (Figures 4A and 4B). Gene Ontology (GO) enrichment analysis revealed that most of the upregulated GO terms enriched in the mat *ΔIG* LSK were related to proliferation, growth, development, and metabolism (Figure 4C; Table S4), suggesting that hyperactive proliferation and metabolism might be responsible for HSC deficiency in mat *ΔIG* mutants. Two terms ("regulation of cellular response to insulin stimulus" and "positive regulation of PI3K cascade") were upregulated in mat *ΔIG*, leading us to hypothesize that the PI3K-mTOR pathway might be hyperactivated in mat *ΔIG* HSCs. The PI3K-mTOR pathway is known to contribute to hematopoiesis, with downregulation of mTORC1 being essential for HSC self-renewal and maintenance, whereas abnormal activation of mTOR signaling is usually associated with leukemogenesis (Chen et al., 2008; Hirao and Hoshii, 2013; Lee et al., 2010). Furthermore, our previous study showed that activation of PI3K-AKT by PTEN mutation led to HSC exhaustion (Zhang et al., 2006). To test our hypothesis, we conducted three individual sets of experiments. First, to detect phospho (p)-Akt^{S473} and p-mTOR^{S2448} activities in fetal liver HSCs, we performed immunostaining on sorted fetal liver LSK cells. Quantification of staining intensity revealed that, compared to control, mat *ΔIG* exhibited 1.2-fold, 2-fold, and 1.9-fold increased activity of p-Akt^{S473}, p-mTOR^{S2448}, and p-S6$^{S235/236}$, respectively (Figures 4D–4G; Figures S4A and S4B). Second, to determine PI3K-mTOR activities, we performed intracellular flow cytometry and observed that median fluorescence intensities (MFIs) of p-Akt^{S473}, p-Akt^{S308}, and p-mTOR^{S2448} were higher in LSK and HSCs, but not in progenitor and lineage cells, in mat *ΔIG* compared to WT (Figures 4H, 4I, and S4C). We also observed a significant increase in MFI of p-mTOR^{S2481}, indicating that both mTORC1 and mTORC2 were hyperactivated in mat *ΔIG* (Figure S4D). However, we observed no significant difference in MFIs of LKB1, p-AMPKα^{T172}, p-FoxO1^{T24}/FoxO3a^{T32}, or p-SGK1^{S78} (Figures S4E–S4H). Third, to test PI3K-mTOR activities in adult HSCs, we performed flow cytometry in recipient BM cells. Interestingly, MFIs of p-Akt^{S473} and p-mTOR^{S2448} in donor CD49b^{lo} HSCs were 145% and 133% higher, respectively, in mat *ΔIG* than in WT (Figures 4J and 4K). Taken together, these data suggest that loss of imprinting at the *Dlk1-Gtl2* locus induces hyperactivation of the PI3K-mTOR pathway in both fetal liver HSCs and adult donor HSCs.

miRNAs in the *Gtl2* Locus Suppressed Multiple Components of the PI3K-mTOR Pathway

Based on our RNA-seq data that the small ncRNAs were exclusively enriched in CD49b^{lo} HSCs together with *Gtl2* (Figure 1F), we reasoned that these small ncRNAs might contribute to the hyperactivation of PI3K-mTOR signaling in the mutant HSCs. To test this idea, we performed small RNA-seq in both fetal liver HSCs and adult HSCs (Figure 5A). Intriguingly, we observed that small ncRNAs in the *Gtl2* locus showed a widespread decrease in mat *ΔIG* fetal liver HSCs and exhibited an obvious enrichment in CD49b^{lo} HSCs relative to other adult HSPCs (Figures 5B and 5C). Moreover, ncRNAs in fetal liver HSCs and adult CD49b^{lo} HSCs showed striking similarity, suggesting that these ncRNAs might be specifically processed in HSCs. Combining the ncRNAs downregulated in mat *ΔIG* and

upregulated in CD49b^{lo}, we identified 15 miRNAs and 10 snoRNAs that might be responsible for HSC deficiency and PI3K-mTOR pathway hyperactivation (Figure 5D; Table S5).

Compared to snoRNAs, which function to methylate rRNA and snRNA (Cavaillé et al., 1996), miRNAs are widely reported to repress translation or trigger mRNA degradation by recognizing complementary target sites in the 3′ UTRs of cognate mRNAs (Bartel, 2009). We used TargetScan 6.2 to predict which components in the PI3K-mTOR pathway might be targeted by these miRNAs (Figure 5E). Unexpectedly, 21 genes distributed over the entire PI3K-mTOR pathway contain one or multiple conserved binding sites of *Gtl2*-derived miRNAs in their respective 3′ UTRs (Figure 5F). We then used luciferase reporter assays to determine whether the corresponding mRNAs involved in the mTOR pathway were direct targets of these miRNAs. We first cloned full-length fragments of their 3′ UTRs into the luciferase reporter plasmid psi-CHECK2. Then we transfected either a mature miRNA duplex or a negative control with cognate 3′ UTR constructs into HEK293T cells and found that most of these miRNAs significantly repressed the relative luciferase activities of the 3′ UTRs of IGF1, IGF1R, IRS1, PIK3R1, AKT1, RHEB, RPTOR, PGC-1α, RPS6KB1, and EIF4E (Figure 5G). Moreover, mutation of cognate miRNA binding sites in the 3′ UTRs of RHEB and AKT1 abrogated their repression (Figures S5A and S5B). Further, we infected mouse MEF cells with lentiviruses that overexpress individual miRNAs. Our western blot data showed that miRNAs in the *Gtl2* locus could repress expression of AKT1 and RPTOR at protein levels (Figures 5H and 5I). We also measured expression levels of AKT1 and RPTOR in HSCs and found that these were markedly higher in both fetal liver HSCs and donor CD49b^{lo} HSCs of mat *ΔIG* compared to WT (Figures S5C–S5F). Together, these data indicate that multiple components of the PI3K-mTOR pathway are de novo and direct targets of miRNAs derived from the *Gtl2* locus.

To assess whether the HSC deficiency in mat *ΔIG* was due to downregulation of these miRNAs, we individually cloned 10 highly expressed miRNAs within this locus into lentiviral vectors and infected sorted fetal liver LSK cells with a pool of lentiviruses (Figure 5J). 16 weeks posttransplantation, we found that the repopulation rate and absolute number of donor CD49b^{lo} HSCs in mat *ΔIG* HSCs were increased 2.9-fold and 5.7-fold, respectively, compared to WT HSCs after overexpression of these miRNAs. This implies that miRNAs in the *Gtl2* locus are likely responsible for the HSC deficiency in mat *ΔIG* (Figures 5K and 5L).

Loss of Imprinting at the *Dlk1-Gtl2* Locus Enhanced Mitochondrial Biogenesis, Metabolic Activity, and ROS Levels in HSCs

The PI3K-mTOR pathway serves as a sensor to integrate various environmental cues, such as nutrition and growth factors (Laplante and Sabatini, 2012). mTOR not only stimulates de novo synthesis of primary biosynthetic products such as proteins, nucleotides, and lipids, but also produces ATP by either enhancing mitochondrial activity through 4E-BP-dependent translational regulation (Morita et al., 2013) or activating PGC-1α, a master transcription regulator in the mitochondrial biogenic regulatory cascade (Cunningham et al., 2007). Since PGC-1α and EIF4E were directly targeted by miRNAs in the *Gtl2* locus, we examined their

expression in mat *ΔIG* HSCs. Indeed, we found MFIs of PGC-1α and p-4E-BP1$^{T37/46}$ in both fetal liver and donor CD49b^{lo} HSCs to be significantly increased in mat *ΔIG* (Figures 6A–6D).

We then measured mitochondrial properties in fetal liver HSCs. Using flow cytometry with MitoTracker Green and DilC5, we observed a significant increase in mitochondrial mass and mitochondrial membrane potential (Δψ) in HSPCs of mat *ΔIG* (Figures 6E and 6F). Also, the mtDNA copy number increased markedly in mat *ΔIG* LSK cells, but not in Lin$^+$ cells, compared to control (Figure 6G). Moreover, using transmission electron microscopy (TEM) technology to measure the morphology of mitochondrion, we observed increased mitochondrial number and folds of cristae in mat *ΔIG* HSCs (Figures 6H and 6I). Mitochondria constitute the most prominent source of ATP production mainly through the Krebs cycle and oxidative phosphorylation (OXPHOS) (Fernie et al., 2004). Thus, we next investigated glucose metabolism in mat *ΔIG* mutants. By performing flow cytometry with 2-NBDG, a fluorescent glucose analog, we found increased glucose uptake in HSPCs of mat *ΔIG* (Figure 6J). Finally, we found greatly increased basal ATP levels in fetal liver LSK cells, but not in Lin$^+$ cells, in mat *ΔIG* compared to contol (Figure 6K). In contrast, there was no difference in either mitochondrial activity or metabolism between pat *ΔIG* mutants and control (Figures S6A–S6D).

A hyperactive mTOR activity correlates with a high level of ROS (Jang and Sharkis, 2007). We next measured ROS levels using 2′,7′-dichlorodihydro-fluorescein diacetate (H2-DCFDA) and observed markedly increased ROS levels in HSPCs of mat *ΔIG* (Figure 6L), consitent with a previous study using a similar mouse model, *TSC1*$^{-/-}$ (Chen et al., 2008). We next measured apoptosis in fetal liver HSCs and found a significantly higher percentage of apoptotic cells in HSPCs of mat *ΔIG* than of WT, which to a certain extent explains the reduced HSPC number in mat *ΔIG* (Figure 6M).

To further investigate the role of the *Dlk1-Gtl2* locus in mitochondrial metabolism and ROS levels, we performed metabolic assays in mat *ΔGtl2* mutants. We found that compared to control, HSPCs in the mat *ΔGtl2* fetal livers exhibited increased mitochondrial mass, Δψ, glucose uptake, oxygen consumption rate, ROS levels, and apoptosis (Figures S6E–S6J). These findings support the likelihood that loss of imprinting at the *Dlk1-Gtl2* locus leads to enhanced mitochondrial biogenesis, metabolic activity, and increased ROS levels in HSCs.

Pharmacological Inhibition of the PI3K-mTOR Pathway or ROS Production Partially Rescued HSC Deficiency in mat Δ*IG* Mutants

Given that loss of imprinting at the *Dlk1-Gtl2* locus activates the PI3K-mTOR pathway and enhances mitochondrial biogenesis, metabolic activity, and ROS production, we asked whether pharmacological inhibition of either the PI3K-mTOR pathway or ROS production could abrogate the HSC defect caused by the *Dlk1-Gtl2* locus deletion. We first transplanted sorted HSCs from WT and mat *ΔIG* fetal livers into lethally irradiated recipient mice. After stabilization of donor BM cells, we administered vehicle control or rapamycin, which interacts with peptidylproline isomerase FKBP12 and specifically inhibits mTORC1 activity, to the recipients daily (Figure 7A). Indeed, we found that the repopulation rate after rapamycin treatment in mat *ΔIG* HSCs was 715% higher compared to only 45.9% higher in

WT HSCs (Figure 7B). Likewise after rapamycin treatment, the absolute number of donor CD49b^{lo} HSCs in mat *ΔIG* was 311.5% higher compared to only 60.4% higher in WT mice (Figure 7C). Intracellular immunostaining revealed that rapamycin significantly reduced MFIs of p-mTOR^{S2448}, p-4E-BP1$^{T37/46}$, and PGC-1α in donor CD49b^{lo} HSCs, supporting a decrease in mTORC1 activity following rapamycin administration (Figures 7D, S7A, and S7B). Furthermore, rapamycin clearly restored the mitochondrial mass, glucose uptake rate, percentage of G0 phase, and ROS levels in donor CD49b^{lo} HSCs (Figures 7E–7H). To further confirm that a hyperactivated PI3K-mTOR pathway led to HSC deficiency, we treated recipient mice with several different PI3K-mTOR pathway inhibitors, NVP-BEZ235 (dual PI3K and mTOR inhibitor), PP242 (mTOR inhibitor), or MK-2206 (pan AKT inhibitor). Our transplantation data revealed that the decreased repopulation rates in mat *ΔIG* were abrogated at varying levels by administration of these inhibitors (Figures S7C and S7D). We next tested whether inhibition of ROS production could abrogate the HSC defects. We transplanted whole fetal liver cells into lethally irradiated recipient mice and fed them with water containing N-acetyl cysteine (NAC), an antioxidant to scavenge free radicals (Figure 7I). Intriguingly, we found that NAC treatment not only reduced ROS levels, but also partially restored the repopulation rate and absolute numbers of donor CD49b^{lo} HSCs in mat *ΔIG* (Figures 7J–7L). Overall, these data show that inhibiting either the PI3K-mTOR pathway or ROS production partially restores the HSC deficiency in mat *ΔIG* mutants.

DISCUSSION

In this study, by using global transcription profiling, we identified unique fingerprint lncRNAs in 17 hematopoietic cell types, in which lncRNAs in the *Dlk1-Gtl2* locus were predominantly enriched in CD49b^{lo} LT-HSCs. Deletion of either *IG-DMR* or *Gtl2* from the maternally inherited allele led to downregulation of *Gtl2* and the downstream miRNA mega-cluster, activation of the PI3K-mTOR pathway, enhanced mitochondrial biogenesis, enhanced metabolic activity, and increased ROS levels, eventually leading to HSC apoptosis (Figure 7M).

Specific Expression of lncRNAs in Hematopietic Stem, Progenitor, and Lineage Cells

Recent studies have revealed critical roles of epigenetic regulation in HSCs, including ncRNAs, DNA methylation, and histone modification (Cullen et al., 2014; Luo et al., 2015). Our study, using 17 hematopoietic stem, progenitor, and lineage cells, systematically identified unique fingerprints of lncRNAs, opening the opportunity to investigate the roles and underlying molecular mechanisms of lncRNAs in each cell type. From this framework, using unsupervised hierarchical cluster analysis and PCA on lncRNAs, we revealed that CD49b^{lo} HSCs stand at the apex of the hematopoietic hierarchy, and lncRNAs from the *Dlk1-Gtl2* locus were predominantly enriched in the CD49b^{lo} HSCs.

ncRNAs from the Gtl2 Imprinting Locus Link Fetal Liver HSCs to Adult LT-HSCs and Function to Maintain LT-HSCs

A known feature of fetal HSCs distinctive from adult HSCs is their cycling status. The reason why functionality of adult stem cells, but not fetal HSCs, is associated with quiescent status has been elusive. It is therefore striking to find a link between fetal liver HSCs and the

adult CD49b^{lo} LT-HSCs in that they exhibit similar ncRNA expression patterns, particularly the ncRNAs from the maternally inherited allele in the *Dlk1-Gtl2* locus (Figure 2B), suggesting that these *Gtl2*-derived ncRNAs play a role in maintaining both fetal and adult HSCs. Indeed, our study provides direct evidence that the *Dlk1-Gtl2* locus is required for preservation of HSCs: loss of either mat *ΔIG* or *Gtl2* per se in HSCs led to impaired HSC long-term reconstitution capacity. Consistent with previous studies that show that metabolic properties correlate with HSC functionality (Simsek et al., 2010; Suda et al., 2011; Takubo et al., 2013), our data further elucidate the role of the *Dlk1-Gtl2* locus in preserving both fetal HSCs and adult LT-HSCs by inhibiting the PI3K-mTOR pathway and restricting mitochondrial metabolism.

An miRNA Mega-Cluster in the *Gtl2* Locus Controls Mitochondrial Biogenesis and Metabolic Activity via Inhibiting the mTOR Pathway

The *Dlk1-Gtl2* locus contains the largest cluster of miRNAs in the mammal genome and a large cluster of C/D box snoRNAs. A recent study revealed that Polycomb Repressive Complex 2 (PRC2) transcriptionally regulates the *Gtl2* locus through DNA methylation at *IG-DMR* (Das et al., 2015). In this study, our RNA-seq data showed that these small ncRNAs were simultaneously expressed with *Gtl2*, supporting the hypothesis that these ncRNAs are transcribed as a large polycistronic transcription unit (Seitz et al., 2004; Tierling et al., 2006). Recent studies have linked the *Dlk1-Gtl2* locus to energy metabolism. In one study, the *Dlk1-Gtl2* locus was reported to be crucial for the transition to postnatal life by converging on the development of brown fat (Charalambous et al., 2012). In another study using a mouse model with the entire miR-379/miR-410 cluster deleted, researchers found that this cluster could control neonatal metabolic adaptation (Labialle et al., 2014). Consistently, our data reveal that deletion of either *IG-DMR* or *Gtl2* in HSCs leads to downregulation of *Gtl2* and the downstream miRNA mega-cluster and enhanced mitochondrial biogenesis and metabolic activity.

An interesting recent study showed that the mTOR pathway controls the transition from G_0 to G_{Alert} phase in quiescent stem cells, which functions as an “alerting” mechanism to enhance tissue regenerative function (Rodgers et al., 2014). Our study further reveals that the miRNA mega-cluster in the *Gtl2* locus suppresses the entire PI3K-mTOR pathway and inhibits mitochondrial biogenesis and metabolic activity, suggesting the essential roles of metabolic states in preserving LT-HSCs.

EXPERIMENTAL PROCEDURES

Mice

All mice used in this study were housed in the AAALAC-accredited animal facility at the Stowers Institute for Medical Research (SIMR) and handled according to SIMR and National Institutes of Health guidelines. All procedures involving experimental animals were approved by the Institutional Animal Care and Use Committee (IACUC) of SIMR. C57BL/6, *Ptprc*, and *Dlk1* floxed mice were purchased from Jackson Laboratory.

RNA-Seq

Total RNA was isolated using Trizol (Invitrogen). Sequencing libraries were prepared from 10–100 ng total RNA using the TruSeq RNA Sample Preparation Kit v2 (Illumina).

Intracellular Flow Cytometry

Cells from E15.0 fetal livers or recipient BM were initially stained with surface markers for 30–60 min at 4°C and washed with PBS (2% FBS). Cells were then fixed and permeabilized with Cytofix/Cytoperm buffer (BD Biosciences) for 30 min and stained on ice with individual primary antibody or isotype control for 30 min. Samples were then incubated with fluorescent dye conjugated secondary antibodies (Molecular Probes) for 30 min and analyzed by flow cytometry. FlowJo software was used to calculate the MFI for each sample.

Luciferase Reporter Assay

HEK293T cells (5×10^4/well) were seeded into 24-well plates 1 day before transfection. 200 ng of each 3′ UTR construct was co-transfected with 20 nM miRNA mimics or scramble control using Lipofectamine 2000 (Invitrogen) following the manufacturer's instructions. Cells were harvested 48 hr after transfection, and then Firefly and Renilla luciferase activities were measured using the dual-luciferase reporter kit (Promega) on Victor3 Multilabel Plate Counter (Perkin Elmer).

Statistics

Values are shown as the mean ± SD or SEM as indicated. All statistical analyses were generated using GraphPad Prism 5 (GraphPad Software). Student's t test was used for comparisons between two groups, whereas one-way ANOVA followed by Tukey's post hoc tests and two-way ANOVA analysis followed by Bonferroni's post hoc tests were used for comparisons among multiple groups. Log rank (Mantel-Cox) test was used for Kaplan-Meier survival. Statistical significance was defined as $p < 0.05$.

Supplementary Material

Refer to Web version on PubMed Central for supplementary material.

Acknowledgments

We thank M. Miller for model image modification; K. Tannen for proofreading and editing; and M. Hembree, H. Marshall, K. Zapien, D. Dukes, C. Semerad, A. Box, J. Park, L. Blunk, A. Perera, and A. Peak for technical support. We are grateful to Linheng Li laboratory members for scientific discussion and critical reading of the manuscript. This work was funded by the Stowers Institute for Medical Research and the American Society of Hematology (ASH) Scholar Award. L.Z. was supported by the National Natural Science Foundation of China (31200575) and the Natural Science Foundation of Tianjin (12JCQNJC07600).

References

Alvarez-Dominguez JR, Hu W, Yuan B, Shi J, Park SS, Gromatzky AA, van Oudenaarden A, Lodish HF. Global discovery of erythroid long noncoding RNAs reveals novel regulators of red cell maturation. Blood. 2014; 123:570–581. [PubMed: 24200680]

Bartel DP. MicroRNAs: target recognition and regulatory functions. Cell. 2009; 136:215–233. [PubMed: 19167326]

Bartolomei MS. Genomic imprinting: employing and avoiding epigenetic processes. Genes Dev. 2009; 23:2124–2133. [PubMed: 19759261]

Beerman I, Bhattacharya D, Zandi S, Sigvardsson M, Weissman IL, Bryder D, Rossi DJ. Functionally distinct hematopoietic stem cells modulate hematopoietic lineage potential during aging by a mechanism of clonal expansion. Proc Natl Acad Sci USA. 2010; 107:5465–5470. [PubMed: 20304793]

Benveniste P, Frelin C, Janmohamed S, Barbara M, Herrington R, Hyam D, Iscove NN. Intermediate-term hematopoietic stem cells with extended but time-limited reconstitution potential. Cell Stem Cell. 2010; 6:48–58. [PubMed: 20074534]

Berg JS, Lin KK, Sonnet C, Boles NC, Weksberg DC, Nguyen H, Holt LJ, Rickwood D, Daly RJ, Goodell MA. Imprinted genes that regulate early mammalian growth are coexpressed in somatic stem cells. PLoS ONE. 2011; 6:e26410. [PubMed: 22039481]

Cavaillé J, Nicoloso M, Bachellerie JP. Targeted ribose methylation of RNA in vivo directed by tailored antisense RNA guides. Nature. 1996; 383:732–735. [PubMed: 8878486]

Charalambous M, Ferron SR, da Rocha ST, Murray AJ, Rowland T, Ito M, Schuster-Gossler K, Hernandez A, Ferguson-Smith AC. Imprinted gene dosage is critical for the transition to independent life. Cell Metab. 2012; 15:209–221. [PubMed: 22326222]

Chen C, Liu Y, Liu R, Ikenoue T, Guan KL, Liu Y, Zheng P. TSC-mTOR maintains quiescence and function of hematopoietic stem cells by repressing mitochondrial biogenesis and reactive oxygen species. J Exp Med. 2008; 205:2397–2408. [PubMed: 18809716]

Cullen SM, Mayle A, Rossi L, Goodell MA. Hematopoietic stem cell development: an epigenetic journey. Curr Top Dev Biol. 2014; 107:39–75. [PubMed: 24439802]

Cunningham JT, Rodgers JT, Arlow DH, Vazquez F, Mootha VK, Puigserver P. mTOR controls mitochondrial oxidative function through a YY1-PGC-1alpha transcriptional complex. Nature. 2007; 450:736–740. [PubMed: 18046414]

da Rocha ST, Edwards CA, Ito M, Ogata T, Ferguson-Smith AC. Genomic imprinting at the mammalian Dlk1-Dio3 domain. Trends Genet. 2008; 24:306–316. [PubMed: 18471925]

Das PP, Hendrix DA, Apostolou E, Buchner AH, Canver MC, Beyaz S, Ljuboja D, Kuintzle R, Kim W, Karnik R, et al. PRC2 Is Required to Maintain Expression of the Maternal Gtl2-Rian-Mirg Locus by Preventing De Novo DNA Methylation in Mouse Embryonic Stem Cells. Cell Rep. 2015; 12:1456–1470. [PubMed: 26299972]

Ferguson-Smith AC. Genomic imprinting: the emergence of an epigenetic paradigm. Nat Rev Genet. 2011; 12:565–575. [PubMed: 21765458]

Fernie AR, Carrari F, Sweetlove LJ. Respiratory metabolism: glycolysis, the TCA cycle and mitochondrial electron transport. Curr Opin Plant Biol. 2004; 7:254–261. [PubMed: 15134745]

Ferrón SR, Charalambous M, Radford E, McEwen K, Wildner H, Hind E, Morante-Redolat JM, Laborda J, Guillemot F, Bauer SR, et al. Postnatal loss of Dlk1 imprinting in stem cells and niche astrocytes regulates neurogenesis. Nature. 2011; 475:381–385. [PubMed: 21776083]

Haug JS, He XC, Grindley JC, Wunderlich JP, Gaudenz K, Ross JT, Paulson A, Wagner KP, Xie Y, Zhu R, et al. N-cadherin expression level distinguishes reserved versus primed states of hematopoietic stem cells. Cell Stem Cell. 2008; 2:367–379. [PubMed: 18397756]

Hirao A, Hoshii T. Mechanistic/mammalian target protein of rapamycin signaling in hematopoietic stem cells and leukemia. Cancer Sci. 2013; 104:977–982. [PubMed: 23648144]

Jang YY, Sharkis SJ. A low level of reactive oxygen species selects for primitive hematopoietic stem cells that may reside in the low-oxygenic niche. Blood. 2007; 110:3056–3063. [PubMed: 17595331]

Labialle S, Marty V, Bortolin-Cavaillé ML, Hoareau-Osman M, Pradère JP, Valet P, Martin PG, Cavaillé J. The miR-379/miR-410 cluster at the imprinted Dlk1-Dio3 domain controls neonatal metabolic adaptation. EMBO J. 2014; 33:2216–2230. [PubMed: 25124681]

Laplante M, Sabatini DM. mTOR signaling in growth control and disease. Cell. 2012; 149:274–293. [PubMed: 22500797]

Lee JY, Nakada D, Yilmaz OH, Tothova Z, Joseph NM, Lim MS, Gilliland DG, Morrison SJ. mTOR activation induces tumor suppressors that inhibit leukemogenesis and deplete hematopoietic stem cells after Pten deletion. Cell Stem Cell. 2010; 7:593–605. [PubMed: 21040901]

Li L, Clevers H. Coexistence of quiescent and active adult stem cells in mammals. Science. 2010; 327:542–545. [PubMed: 20110496]

Lin SP, Youngson N, Takada S, Seitz H, Reik W, Paulsen M, Cavaille J, Ferguson-Smith AC. Asymmetric regulation of imprinting on the maternal and paternal chromosomes at the Dlk1-Gtl2 imprinted cluster on mouse chromosome 12. Nat Genet. 2003; 35:97–102. [PubMed: 12937418]

Lin SP, Coan P, da Rocha ST, Seitz H, Cavaille J, Teng PW, Takada S, Ferguson-Smith AC. Differential regulation of imprinting in the murine embryo and placenta by the Dlk1-Dio3 imprinting control region. Development. 2007; 134:417–426. [PubMed: 17166925]

Luo M, Jeong M, Sun D, Park HJ, Rodriguez BA, Xia Z, Yang L, Zhang X, Sheng K, Darlington GJ, et al. Long non-coding RNAs control hematopoietic stem cell function. Cell Stem Cell. 2015; 16:426–438. [PubMed: 25772072]

Morita M, Gravel SP, Chénard V, Sikström K, Zheng L, Alain T, Gandin V, Avizonis D, Arguello M, Zakaria C, et al. mTORC1 controls mitochondrial activity and biogenesis through 4E-BP-dependent translational regulation. Cell Metab. 2013; 18:698–711. [PubMed: 24206664]

Morrison SJ, Hemmati HD, Wandycz AM, Weissman IL. The purification and characterization of fetal liver hematopoietic stem cells. Proc Natl Acad Sci USA. 1995; 92:10302–10306. [PubMed: 7479772]

Randall TD, Lund FE, Howard MC, Weissman IL. Expression of murine CD38 defines a population of long-term reconstituting hematopoietic stem cells. Blood. 1996; 87:4057–4067. [PubMed: 8639761]

Rodgers JT, King KY, Brett JO, Cromie MJ, Charville GW, Maguire KK, Brunson C, Mastey N, Liu L, Tsai CR, et al. mTORC1 controls the adaptive transition of quiescent stem cells from G0 to G(Alert). Nature. 2014; 510:393–396. [PubMed: 24870234]

Seitz H, Royo H, Bortolin ML, Lin SP, Ferguson-Smith AC, Cavaillé J. A large imprinted microRNA gene cluster at the mouse Dlk1-Gtl2 domain. Genome Res. 2004; 14:1741–1748. [PubMed: 15310658]

Simsek T, Kocabas F, Zheng J, Deberardinis RJ, Mahmoud AI, Olson EN, Schneider JW, Zhang CC, Sadek HA. The distinct metabolic profile of hematopoietic stem cells reflects their location in a hypoxic niche. Cell Stem Cell. 2010; 7:380–390. [PubMed: 20804973]

Snyder CM, Rice AL, Estrella NL, Held A, Kandarian SC, Naya FJ. MEF2A regulates the Gtl2-Dio3 microRNA mega-cluster to modulate WNT signaling in skeletal muscle regeneration. Development. 2013; 140:31–42. [PubMed: 23154418]

Suda T, Takubo K, Semenza GL. Metabolic regulation of hematopoietic stem cells in the hypoxic niche. Cell Stem Cell. 2011; 9:298–310. [PubMed: 21982230]

Takahashi N, Okamoto A, Kobayashi R, Shirai M, Obata Y, Ogawa H, Sotomaru Y, Kono T. Deletion of Gtl2, imprinted non-coding RNA, with its differentially methylated region induces lethal parent-origin-dependent defects in mice. Hum Mol Genet. 2009; 18:1879–1888. [PubMed: 19264764]

Takubo K, Nagamatsu G, Kobayashi CI, Nakamura-Ishizu A, Kobayashi H, Ikeda E, Goda N, Rahimi Y, Johnson RS, Soga T, et al. Regulation of glycolysis by Pdk functions as a metabolic checkpoint for cell cycle quiescence in hematopoietic stem cells. Cell Stem Cell. 2013; 12:49–61. [PubMed: 23290136]

Tierling S, Dalbert S, Schoppenhorst S, Tsai CE, Oliger S, Ferguson-Smith AC, Paulsen M, Walter J. High-resolution map and imprinting analysis of the Gtl2-Dnchc1 domain on mouse chromosome 12. Genomics. 2006; 87:225–235. [PubMed: 16309881]

Venkatraman A, He XC, Thorvaldsen JL, Sugimura R, Perry JM, Tao F, Zhao M, Christenson MK, Sanchez R, Yu JY, et al. Maternal imprinting at the H19-Igf2 locus maintains adult haematopoietic stem cell quiescence. Nature. 2013; 500:345–349. [PubMed: 23863936]

Wilson A, Laurenti E, Oser G, van der Wath RC, Blanco-Bose W, Jaworski M, Offner S, Dunant CF, Eshkind L, Bockamp E, et al. Hematopoietic stem cells reversibly switch from dormancy to self-renewal during homeostasis and repair. Cell. 2008; 135:1118–1129. [PubMed: 19062086]

Yang L, Bryder D, Adolfsson J, Nygren J, Månsson R, Sigvardsson M, Jacobsen SE. Identification of Lin(-)Sca1(+)kit(+)CD34(+)Flt3-short-term hematopoietic stem cells capable of rapidly reconstituting and rescuing myeloablated transplant recipients. Blood. 2005; 105:2717–2723. [PubMed: 15572596]

Zacharek SJ, Fillmore CM, Lau AN, Gludish DW, Chou A, Ho JW, Zamponi R, Gazit R, Bock C, Jäger N, et al. Lung stem cell self-renewal relies on BMI1-dependent control of expression at imprinted loci. Cell Stem Cell. 2011; 9:272–281. [PubMed: 21885022]

Zhang J, Grindley JC, Yin T, Jayasinghe S, He XC, Ross JT, Haug JS, Rupp D, Porter-Westpfahl KS, Wiedemann LM, et al. PTEN maintains haematopoietic stem cells and acts in lineage choice and leukaemia prevention. Nature. 2006; 441:518–522. [PubMed: 16633340]

Zhou Y, Cheunsuchon P, Nakayama Y, Lawlor MW, Zhong Y, Rice KA, Zhang L, Zhang X, Gordon FE, Lidov HG, et al. Activation of paternally expressed genes and perinatal death caused by deletion of the Gtl2 gene. Development. 2010; 137:2643–2652. [PubMed: 20610486]

Highlights

- Transcriptome profiling reveals *Gtl2*-derived ncRNA enrichment in LT-HSCs
- Loss of *Dlk1-Gtl2* imprinting leads to functional defects in fetal liver HSCs
- miRNAs of the *Dlk1-Gtl2* locus suppress components of the entire PI3K-mTOR pathway
- PI3K-mTOR inhibition restricts mitochondrial metabolism to preserve LT-HSC function

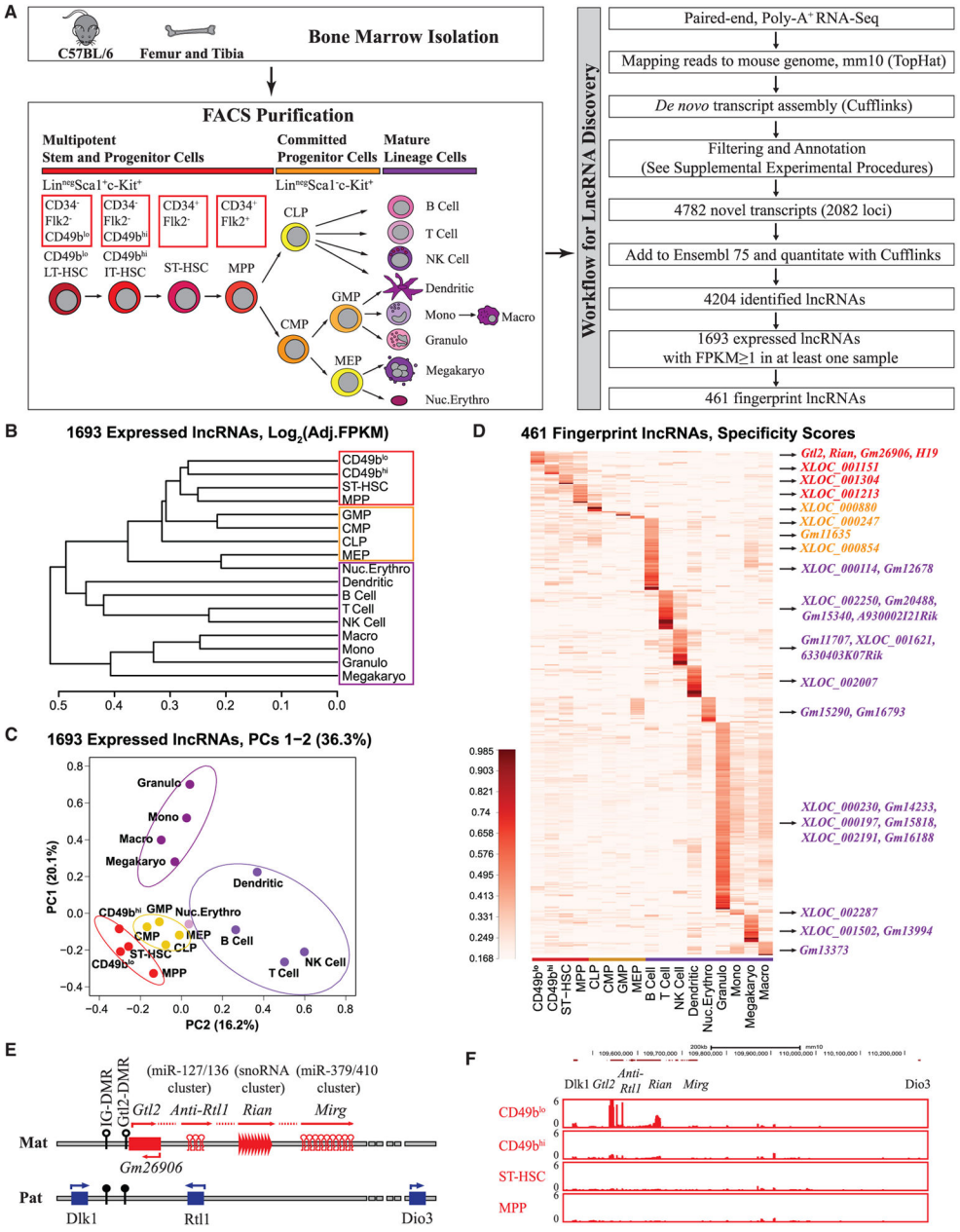

Figure 1. Unique lncRNA Fingerprints in 17 Hematopoietic Cell Types Revealed Enrichment of lncRNAs from the *Dlk1-Gtl2* Locus in CD49b^{lo} LT-HSCs

(A) Schematic representation of the hematopoietic hierarchy showing cell types used in this study and workflow for lncRNA discovery.

(B) A dendrogram displays hierarchical cluster analysis from 1,693 expressed lncRNAs based on Pearson correlations of $\log_2$ (FPKM + 2^{-11}) values. The samples from HSPCs, progenitors, and lineage cells are surrounded by red, yellow, and purple rectangles, respectively.

(C) Population-distance analysis of 1,693 expressed lncRNAs shown in two principal components (PCs 1–2). Cell types are color-coded, labeled by name, and surrounded by

different ellipses. HSPCs, red; committed progenitor cells, yellow; myeloid cells, violet; lymphoid cells, blue; nucleated erythrocytes, pink.

(D) Heat map of cell-type-specific lncRNA fingerprints based on cell specificity scores (color indicates specificity scores; darker corresponds to higher specificity scores). Representative fingerprint lncRNAs in different cell types are shown on the right.

(E) Schematic representation of the *Dlk1-Gtl2* locus. Genes (rectangles) on the maternally inherited allele (in red) and the paternally inherited allele (in blue) are depicted. miRNA and C/D snoRNA genes are shown by hairpin loops and triangles, respectively. Arrows indicate the transcription directions, with the horizontal dash line indicating the hypothesis that *Gtl2, anti-Rtl1, Rian*, and Mirg may constitute a large polycistronic transcription unit. The *IG-DMR* and *Gtl2-DMR* are unmethylated (open circles) on the maternally inherited allele but methylated (filled circles) on the paternally inherited allele.

(F) UCSC Genome Browser images show RNA-seq signal as the density of mapped reads in the whole *Dlk1-Gtl2* locus.

See also Figure S1 and Table S1, Table S2, and Table S3.

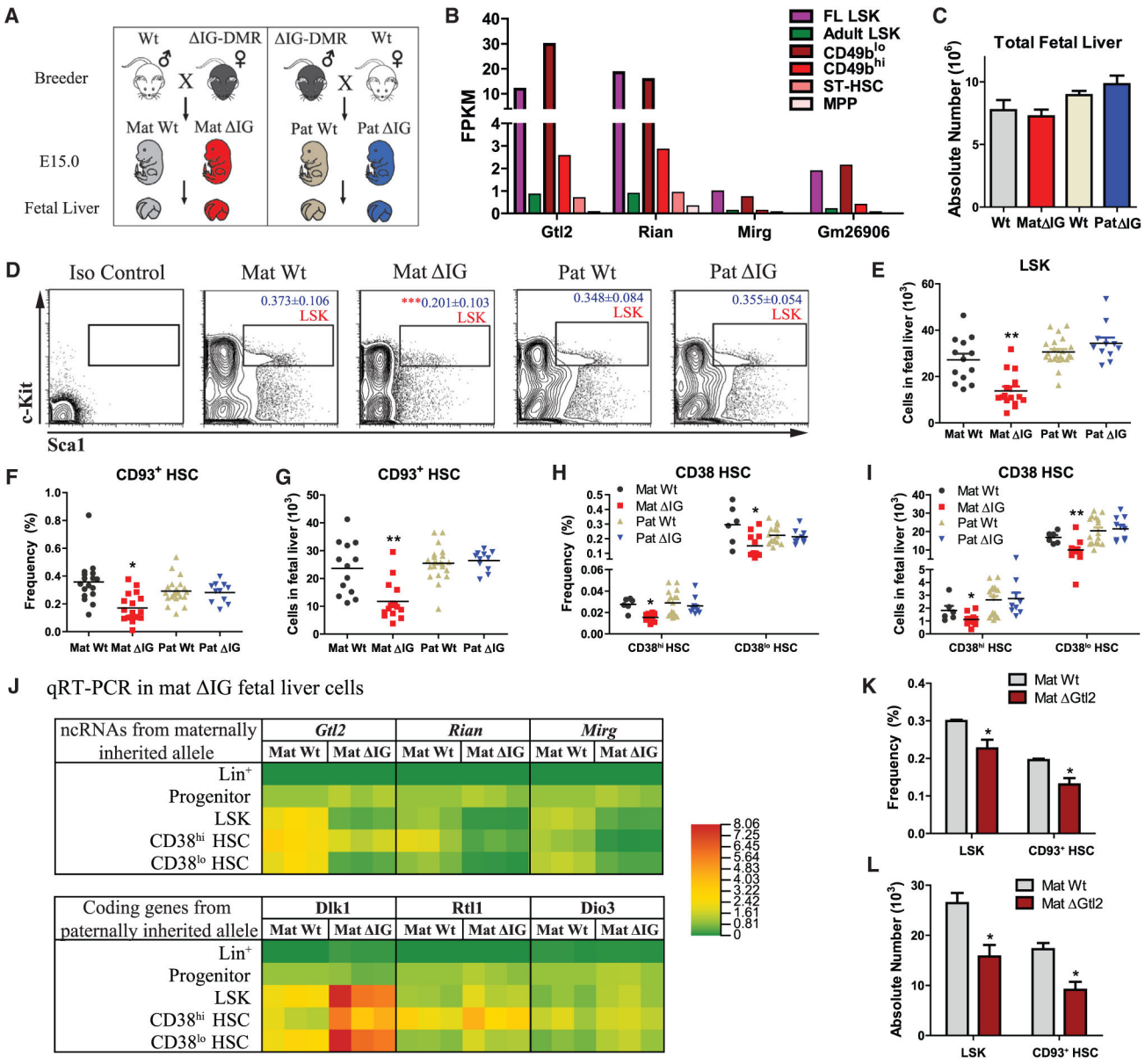

Figure 2. Loss of Imprinting at the *Dlk1-Gtl2* Locus Led to Deficiency in Fetal Liver HSCs

(A) Schematic representation of mating strategy to generate allele-specific mutant embyros.

(B) RNA-seq analysis of lncRNAs in the *Dlk1-Gtl2* locus in E15 fetal liver LSK, adult BM LSK, and four adult HSPC populations.

(C) Absolute numbers of total fetal liver cells (n = 6).

(D–I) Flow cytometric analyses to show the gate, frequency (of total nucleated cells [TNCs]), and absolute numbers of LSK cells, CD93^{+} HSCs, and CD38 HSCs in WT and *ΔIG* fetal liver (n = 6).

(J) Tri-color heat map shows quantitative real-time PCR analysis of *Dlk1-Gtl2* locus genes in HSPCs, progenitors, and lineage cells from WT and mat *ΔIG* fetal livers. *β-Actin* was used as an internal control.

(K and L) Frequency in TNCs and absolute numbers of HSPCs in WT and *ΔGtl2* fetal liver (n = 3). Error bars, SEM; *p < 0.05; **p < 0.01. See also Figure S2 and Table S1, Table S2, and Table S6.

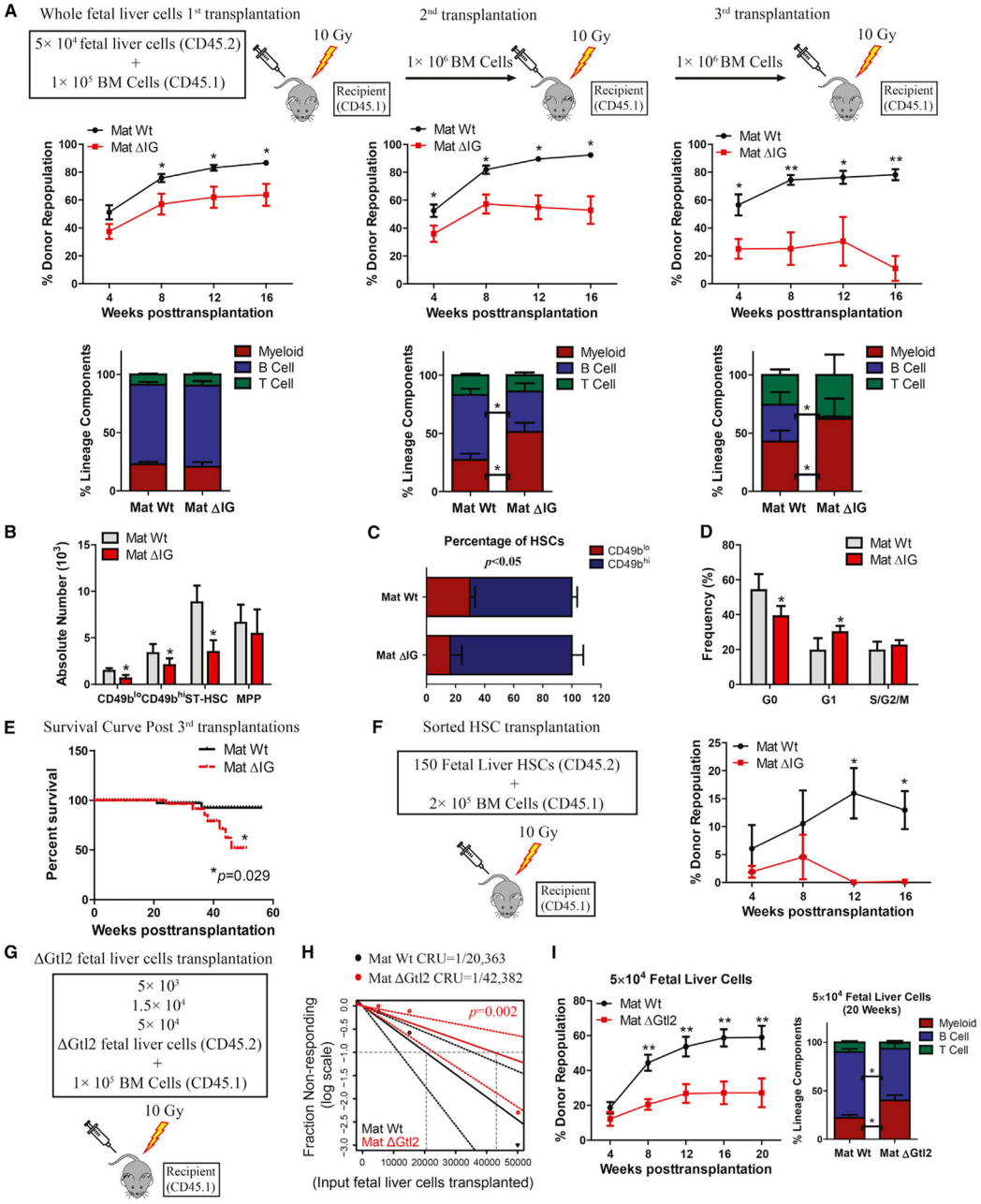

Figure 3. Loss of Imprinting at the *Dlk1-Gtl2* Locus Impaired Long-Term Reconstitution Capacity of Fetal Liver HSCs

(A) 5 × 10^4 WT or mat *ΔIG* fetal liver cells were transplanted with 1 × 10^5 rescue cells into irradiated recipients. At 16 weeks posttransplant, BM isolated from 1st recipients was transplanted into 2nd recipients and, at 16 weeks post 2nd transplant, from 2nd into 3rd recipients at a dosage of 1 ×10^6 cells per mouse. Peripheral blood (PB) was analyzed for percent donor repopulation at the indicated number of weeks after transplants (top panels) and for percent mature donor-derived B, T, and myeloid cells (bottom panels) (n = 10).

(B) Absolute numbers of HSPCs in the BM from 3rd recipients (n = 5).

(C) Percentage of $CD49b^{lo}$ and $CD49b^{hi}$ HSCs in the BM from 3rd recipients (n = 5).

(D) Cell-cycle analysis of CD49b^{lo} HSCs in BM from 1st recipients (n = 5).
(E) Kaplan-Meier survival curve for 1st, 2nd, and 3rd transplant recipients (n = 10).
(F) 150 sorted CD93^{+} HSCs from WT or mat *ΔIG* fetal livers were transplanted with 2 ×10^{5} rescue cells into irradiated recipients. PB analysis for percent engrafted donor cells at the indicated number of weeks posttransplantation is shown.
(G–I) CRU frequency was determined in (H) using ELDA (Extreme Limiting Dilution Analysis). PB of the 5 ×10^{4} group was analyzed for percent donor repopulation at the indicated number of weeks posttransplantation and for percent mature donor-derived B, T, and myeloid cells (I) (n = 10).
Error bars, SD; *p < 0.05; **p < 0.01. See also Figure S3.

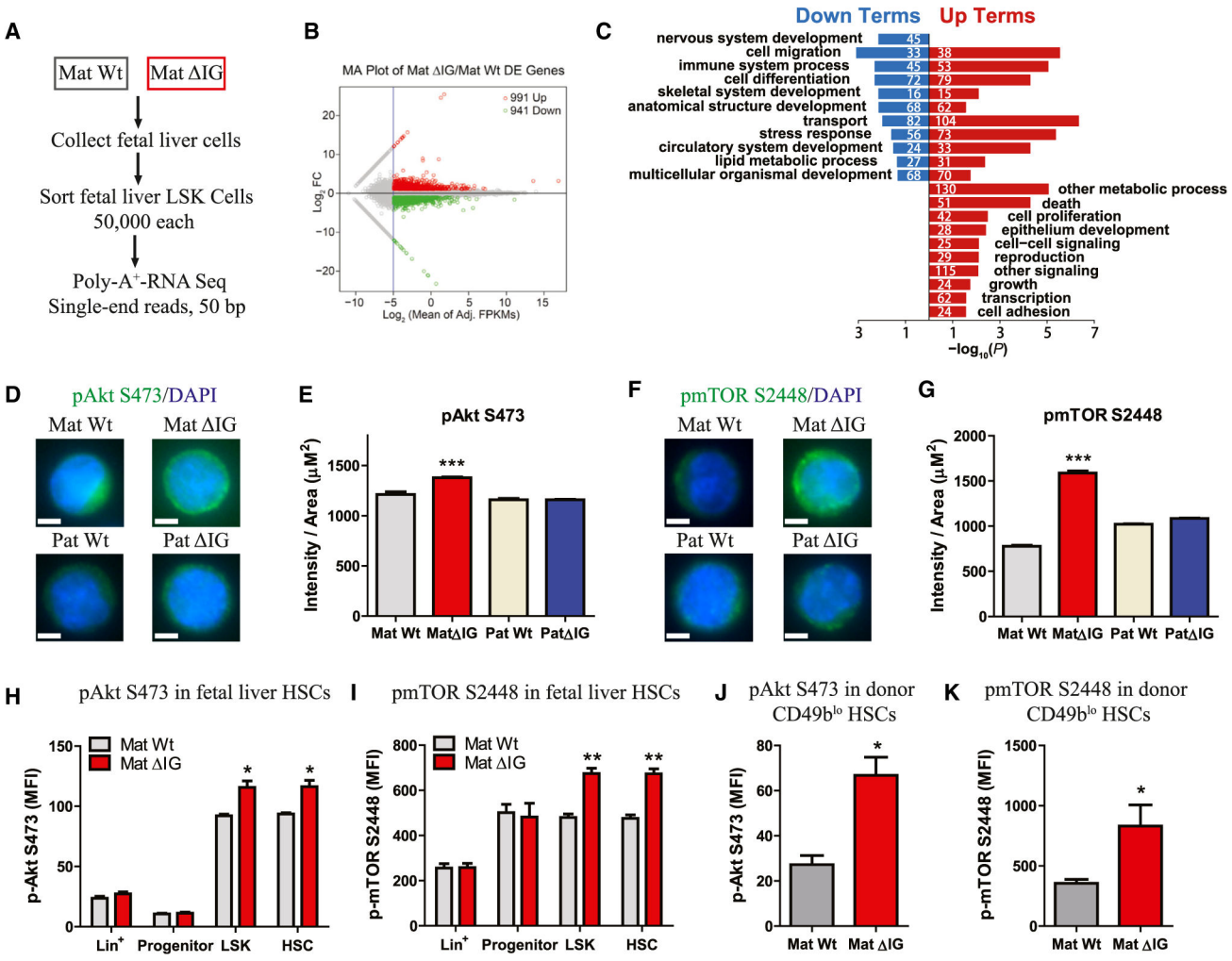

Figure 4. Hyperactivation of the PI3K-mTOR Pathway in mat Δ*IG* Fetal Liver HSPCs

(A) Poly-A$^+$ RNA-seq workflow.

(B) MA plot (plot of mean $\log_2$ difference versus mean $\log_2$ intensity) for differential expression analysis between WT and mat *ΔIG* fetal liver LSK cells.

(C) GO enrichment analysis using $-\log_{10}$ of the uncorrected p value as x axis. The upregulated or downregulated GO terms in mat *ΔIG* are shown in red or blue, respectively. The numbers indicate the amount of enriched genes in each term.

(D–G) Representative image and quantification of staining intensity of LSK cells sorted from WT and *ΔIG* fetal livers for p-Akt^{S473} (n ≥ 43) and p-mTOR^{S2448} (n ≥ 152).

(H–K) MFIs of p-Akt^{S473} and p-mTOR^{S2448} in fetal liver HSCs (H and I, n = 4) and donor CD49b^{lo} HSCs from BM of 3rd recipients (J and K, n ≥ 4).

Error bars, SEM (H and I) or SD. Scale bars, 5 μm. *p < 0.05; **p < 0.01; ***p < 0.001. See also Figure S4, Table S4, and Table S7.

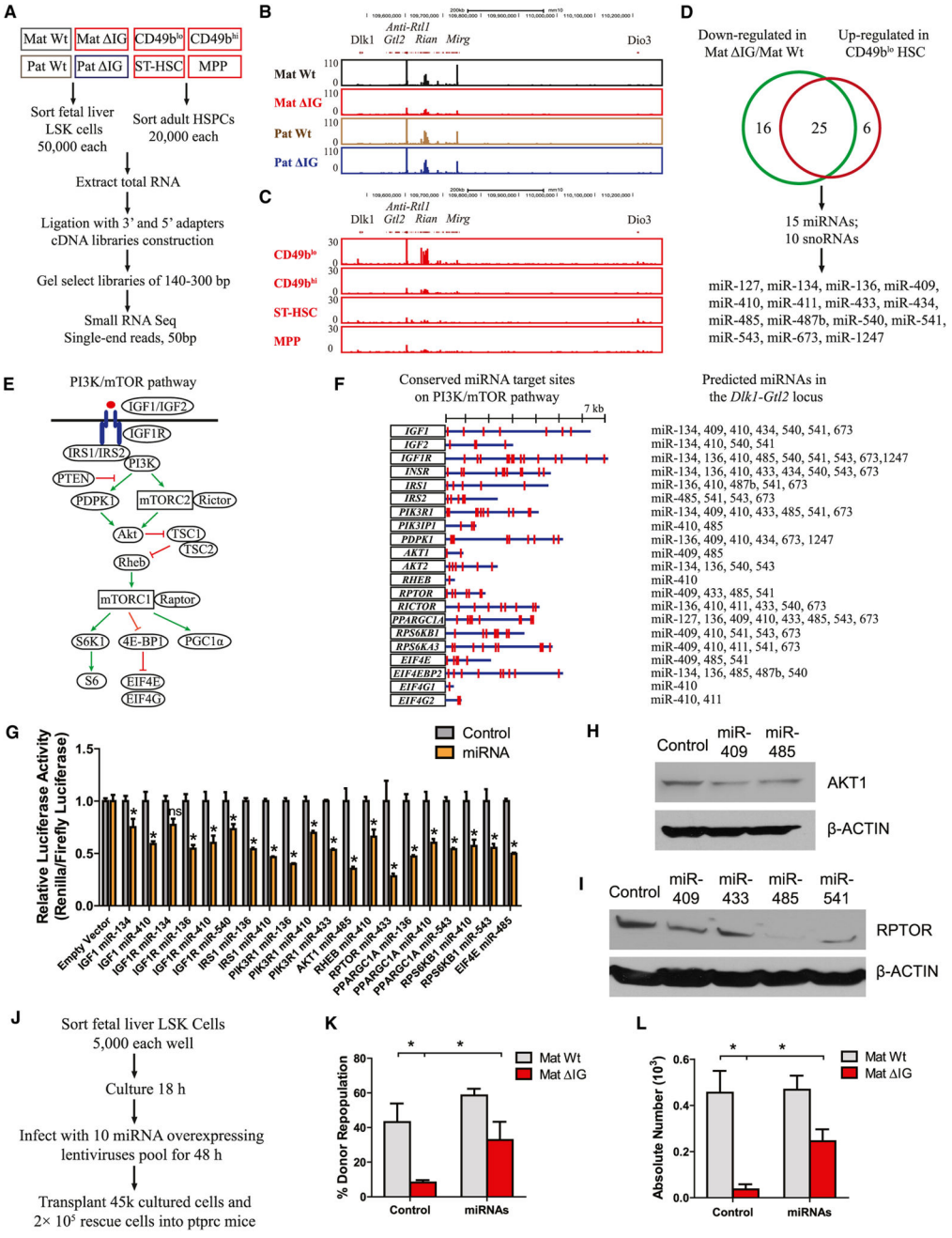

Figure 5. miRNAs in the *Dlk1-Gtl2* Locus Repressed Multiple Components of the PI3K-mTOR Pathway

(A) Small RNA-seq workflow.

(B and C) UCSC Genome Browser images show small RNA-seq signal as the density of mapped reads in the whole *Dlk1-Gtl2* locus from either fetal liver HSCs (B) or adult HSPCs (C).

(D) The Venn diagram shows the overlap between ncRNAs downregulated in mat *ΔIG* and upregulated in CD49b^{lo} HSCs. The miRNAs are listed on the bottom.

(E) Schematic representation of the PI3K-mTOR pathway.

(F) Putative miRNAs and their binding sites in 21 genes of the PI3K-mTOR pathway.
(G) Luciferase reporter assays performed to determine functional miRNA binding sites (n = 2).
(H and I) Western blotting assays performed to detect expression of AKT1 and RPTOR in mouse MEF cells infected with miRNA overexpressing lentivirus. β-ACTIN was used as internal control.
(J) Scheme for transplantation assay rescued by overexpression of 10 miRNAs in *Gtl2* locus.
(K) Quantification of functional HSCs by transplantation assay (n = 6).
(L) Absolute numbers of CD49b^{lo} HSCs in recipient mice at 16 weeks posttransplantation (n = 6).
Error bars, SEM (G) or SD; *p < 0.05; ns, not significant. See also Figure S5 and Table S5, Table S6, and Table S7.

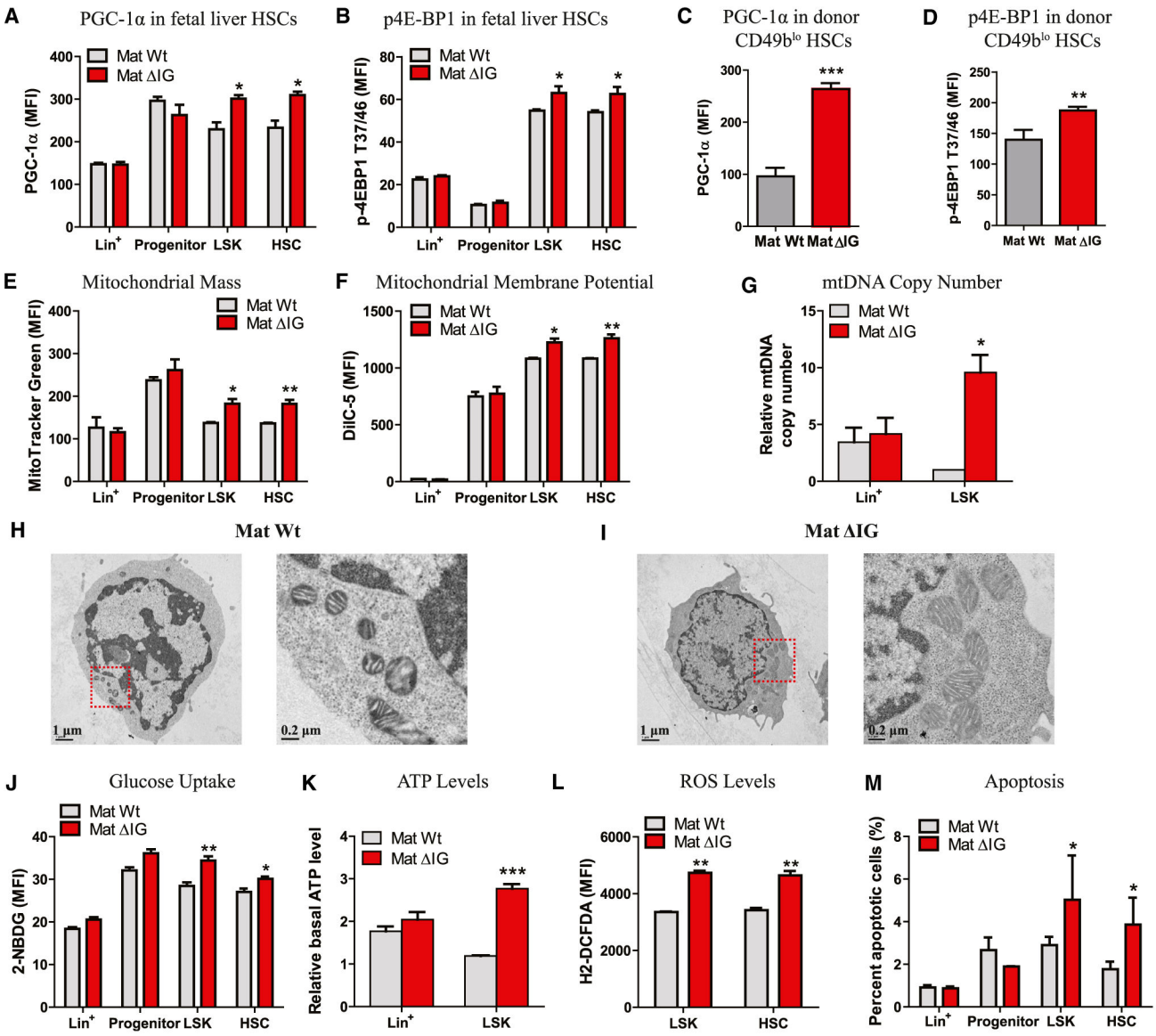

Figure 6. Loss of Imprinting at the *Dlk1-Gtl2* Locus Enhanced Mitochondrial Biogenesis and Metabolic Activity and Increased ROS Levels in HSCs

(A–D) MFI of PGC-1α and p-4E-BP1$^{T37/46}$ in fetal liver HSCs (A and B, n = 3) and donor CD49b^{lo} HSCs from BM of 3rd recipients (C and D, n ≥ 4).

(E) Mitochondrial mass of WT and mat *ΔIG* cells assayed by MitoTracker Green staining (n = 3).

(F) Mitochondrial membrane potential of WT and mat *ΔIG* cells assayed by DilC5 staining (n = 3).

(G) Relative mitochondria DNA copy number of WT and mat *ΔIG* cells assayed by qRT-PCR (n = 2).

(H and I) Representative TEM images of mitochondrial morphology in WT and mat *ΔIG* LSK cells.

(J) Glucose uptake of WT and mat *ΔIG* cells assayed by 2-NBDG (n = 3).

(K) Relative basal ATP levels of WT and mat *ΔIG* cells (n = 2).
(L) ROS levels of WT and mat *ΔIG* cells assayed by H2-DCFDA (n = 3).
(M) Percentage of apoptotic cells in WT and mat *ΔIG* cells assayed by Annexin V and 7-AAD staining (n = 3).
Error bars, SEM or SD (C and D). *p < 0.05; **p < 0.01; ***p < 0.001. See also Figure S6 and Table S7.

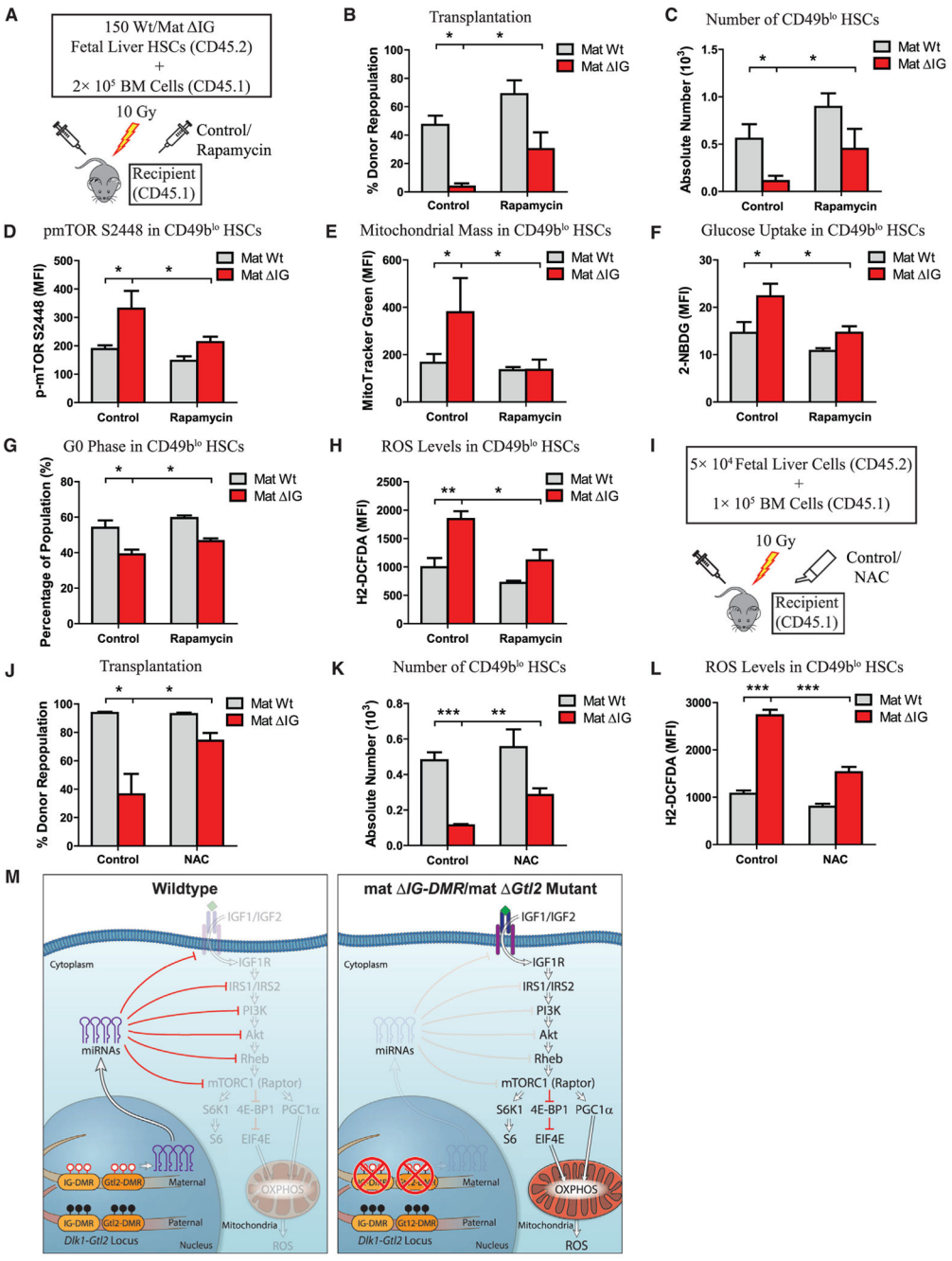

Figure 7. Rapamycin and NAC Partially Rescued Defective HSCs and Metabolic Effects Due to Loss of Imprinting at the *Dlk1-Gtl2* Locus

(A) Scheme for rapamycin administration.

(B) Repopulation assay for rapamycin administration at 12 weeks posttransplantation (n ≥ 4).

(C) Absolute numbers of CD49b^{lo} HSCs in recipient mice with rapamycin administration at 12 weeks posttransplantation (n ≥ 4).

(D) MFI of p-mTOR^{S2448} in donor CD49b^{lo} HSCs from BM of mice treated with rapamycin (n ≥ 4).

(E–H) Mitochondrial mass, glucose uptake, cell-cycle analysis, and ROS levels in donor CD49b^{lo} HSCs from BM of mice treated with rapamycin ($n \geq 4$).

(I) Scheme for NAC administration.

(J) Repopulation assay for NAC administration at 16 weeks posttransplantation ($n = 6$).

(K) Absolute numbers of CD49b^{lo} HSCs in recipient mice fed with NAC water at 16 weeks posttransplantation ($n = 6$).

(L) ROS levels in donor CD49b^{lo} HSCs from BM of mice fed with NAC water ($n = 6$).

(M) Model depicting an essential role of the *Dlk1-Gtl2* locus in preserving HSCs by inhibiting the PI3K-mTOR pathway and restricting mitochondrial metabolism.

Error bars, SD; *$p < 0.05$; **$p < 0.01$; ***$p < 0.001$. See also Figure S7 and Table S7.